Earthquakes and Structures, *Vol. 10, No. 2 (2016) 261-291*
DOI: http://dx.doi.org/10.12989/eas.2016.10.2.261

Influence of infill panels on an irregular RC building designed according to seismic codes

Marianna Ercolino[a], Paolo Ricci[b], Gennaro Magliulo[*] and Gerardo M. Verderame[c]

University of Naples Federico II, Department of Structures for Engineering and Architecture, Via Claudio 21, 80125 Naples, Italy

(Received February 26, 2015, Revised July 8, 2015, Accepted November 6, 2015)

Abstract. This paper deals with the seismic assessment of a real RC frame building located in Italy, designed according to the current Italian seismic code.

The first part of the paper deals with the calibration of the structural model of the investigated building. The results of an in-situ dynamic identification test are employed in a sensitivity and parametric study in order to find the best fit model in terms of frequencies and modal shapes. In the second part, the safety of the structure is evaluated by means of nonlinear static analyses, taking into account the results of the previous dynamic study.

In order to investigate the influence of the infills on the seismic response of the structure, the nonlinear static analyses are performed both neglecting and taking into account the infill panels. The infill panels differently change the behavior of the structure in terms of strength and stiffness at different seismic intensity levels. The assessment study also verifies the absence of brittle failures in structural elements, which could be caused by either the local interaction with infills or the failure of the strength hierarchy.

Keywords: RC frame; dynamic identification; material properties; seismic code; infills; capacity design

1. Introduction

The detailed seismic assessment of real case-study structures provides a precious insight in the investigation of the actual seismic safety obtained when designing structures according to current seismic codes. This allows accounting for complexity and peculiar characteristics of real structures (Fiore *et al*. 2012, Kreslin and Fajfar 2010, Uva *et al*. 2012), often significantly different from theoretical archetype case-study structures, defined based on a simulated design process for scientific research purposes. Nevertheless, such a kind of realistic and detailed assessment depends on the availability of knowledge data.

In this paper, a detailed seismic assessment is carried out on a real RC frame building located

*Corresponding author, Assistant Professor, E-mail: gmagliul@unina.it
[a]Ph.D., E-mail: marianna.ercolino@unina.it
[b]Ph.D., E-mail: paolo.ricci@unina.it
[c]Assistant Professor, E-mail: verderam@unina.it

 ISSN: 2092-7614 (Print), 2092-7622 (Online)

in a high seismic zone in Southern Italy, designed according to the current national seismic code. Complete information is available for the structure: both geometry and reinforcement details and the design process data.

A more reliable knowledge of the structure is also provided by an experimental dynamic identification campaign, aimed at validating the dynamic response of the numerical model. The results of this test allow defining the linear structural model and the material mechanical characteristics.

The actual effect of code provisions on seismic safety is evaluated. At this aim, the seismic capacity assessment is carried out according to a code-like approach, based on Italian and European seismic standards, mostly consistent with each other (Mpampatsikos *et al*. 2008). When this is not possible, for instance when infill elements are considered and code provisions are not adequate, methods and procedures for structural modeling and seismic capacity evaluation from literature are adopted (Dolsek and Fajfar 2004b, Fardis 1997).

The seismic capacity assessment is carried out via nonlinear static analysis, within the N2 method, adopting an incremental approach, which allows the determination of the seismic capacity in terms of a chosen intensity measure of seismic action, corresponding to different performance levels. In this study, Damage Limitation, Significant Damage and Ultimate Limit States are considered. The nonlinear analyses are performed on both bare and infilled structural models in order to also study the influence of the masonry panels on the seismic response at different level of the seismic actions (Limit States).

Both the overstrength of the structural materials and the seismic details can cause a global overstrength of the structure. This effect is evaluated in terms of seismic capacity, i.e., the design seismic spectral acceleration is compared to the spectral accelerations leading to the attainment of different performance levels. Moreover, the effect of the materials overstrength on the safety of the RC elements with respect to shear failure is also assessed. At this aim, the shear strength is compared to the shear strength, obtained with the capacity design rule by considering both the design and median values of the material strength.

The presence of stiff masonry panels in RC frames can cause shear failure in the adjacent columns: the panel transfer additional shear forces to the column at the corner. The assumed nonlinear model of RC members does not take into account the possible shear failure due to the infill influence; moreover, the Italian code does not provide any requirements against this failure. In order to completely define the seismic safety of the case study, the plastic shear in RC members is also compared with the shear due to the infill interaction, according to Eurocode provisions (CEN 2005).

Thus, the results of this realistic and detailed assessment of structural behavior under seismic action, both at local and global level, are illustrated and discussed.

2. Case study building

The building structure consists of a moment resisting frame system (Fig. 1), located in Avellino, Italy (Table 1). The building is part of a more complex residential construction, made up of eight RC structures, divided by structural joints. The main features of the design process and structural characteristics are described in the following paragraphs.

This building is a frame system in longitudinal direction (X) and a dual system in transversal direction (Y) due to the presence of two concrete walls. The design value of the behavior factor

was calculated according to the Italian code. In the two main directions the values were different. On the safe side, the designer adopted the lower value (q=2.88) in both the directions of the structure. This value corresponds to the behavior factor of a wall-equivalent dual system in DC (Ductility Class) "B", irregular in elevation, and it is also consistent with the provisions of the European code (CEN 2005).

The structure has a rectangular shaped plan and it consists of 9 stories, 2 of them are underground stories, with a plan area of about 390 m^2. The height is 3.50 m for the second story and 3.15 m for the other levels. The seismic weight of the building is about 10.6 kN/m^2 at each level, evaluated according to the combination of the seismic action with other loads (CEN 2005).

The building has two 5.70 m bays along the shorter side (*Y* direction in Fig. 2) and seven bays along the longitudinal direction (*X* direction in Fig. 2) with different bay lengths, ranging from 4.40 m to 5.70 m. At the last level the number of bays along *X* is reduced to six.

The floors have a mixed structure characterized by cast-in place concrete, precast joists and hollow bricks, for a total height of 25 cm.

The twenty columns at each level have the same cross-section along the elevation: eight columns have a square cross section (70 cm×70 cm) and twelve columns have a rectangular cross section (40 cm×80 cm). The rectangular columns are arranged with the long side along the *X*-direction, except for one column that is arranged along the *Y* direction, in order to balance the large stiffness in the *Y*-direction due to the presence of the RC structural walls.

The first two underground floors have rectangular beams (40 cm×70 cm) while the other levels have both external rectangular beams (40 cm×60 cm) and internal flat beams with the base width ranging from 65 cm to 95 cm.

Table 1 Seismic hazard parameters: return period (T_R), horizontal peak ground acceleration on stiff soil (a_g), normalized corner period (T_C^*), maximum amplification factor for the horizontal acceleration (F_0); soil type

T_R [yy]	a_g [g]	T_c^* [sec]	F_0 [-]	Soil Type [-]
50	0.0694	0.310	2.321	C
475	0.1935	0.368	2.372	

(a) Under construction (b) Finale state

Fig. 1 The investigated RC structure

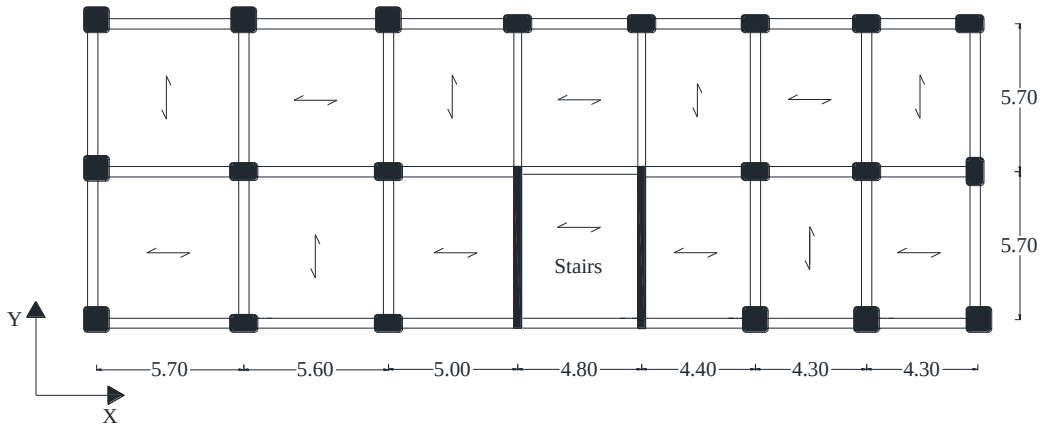

Fig. 2 Plan view of a middle level

Table 2 Minimum and maximum values of the reinforcement percentages in the structural elements

Beams						Columns			
Level	Section	ρ_{min}	ρ_{max}	ρ'_{min}	ρ'_{max}	Level	Section	ρ_{min}	ρ_{max}
I and II	40×70 cm^2	0.36%	0.90%	0.32%	0.79%	All Levels	70×70 cm^2	1.2%	1.4%
All other Level	40×60 cm^2	0.42%	0.90%	0.33%	0.79%		80×40 cm^2	1.0%	1.4%
	Flat beam	0.72%	1.1%	0.72%	1.1%		40×80 cm^2	1.0%	1.4%

Table 3 Summary of the geometrical properties of the infill panels

Type			
	concrete panels	masonry panels	short masonry panels
Thickness	40cm	40cm	40cm
Opening area	None	~(20-30)%	None

The details of the flexural reinforcement for the structural elements are reported in Table 2: for beams ρ and ρ' are the tension and compression longitudinal reinforcement ratio, respectively, while for columns ρ is the total longitudinal reinforcement ratio.

The staircase is reported in Fig. 2 and it is supported by the two concrete walls arranged along the *Y* direction, with a 580 cm×40 cm cross section.

Table 1 shows the seismic hazard parameters for the two design Limit States, namely Damage Limitation and Significant Damage, respectively corresponding to a probability of exceedance of 63% and 10% in 50 years for an ordinary structure, resulting in 50 and 475 years return periods.

The façade or the perimeter of the building comprises of concrete blocks walls at the underground stories and masonry partitions (internal and external) at the upper levels. The geometrical properties of the infill panels (width, thickness, height and area of openings) were directly observed during an in-situ structural survey. A summary is reported in Table 3.

The general arrangement of infills is irregular, both in elevation and in plan, as reported in Fig. 3 for two external frames of the structure. This feature of the structure could cause a weak behavior: the irregular layout of the infills along the height can cause soft story mechanism at the stories with a smaller number of infills, as recorded during some recent seismic events (Kirac *et al*. 2011, Ricci *et al*. 2011a).

The design concrete class is C28/35 (D. M. 14/01/2008 2008b), i.e., the nominal cubic characteristic compressive stress is equal to 35 N/mm^2. The characteristic yielding tensile strength of the reinforcing steel is equal to 450 N/mm^2.

(a) Frontal view (X direction) (b) Lateral view (Y direction)

Fig. 3 External infills distribution

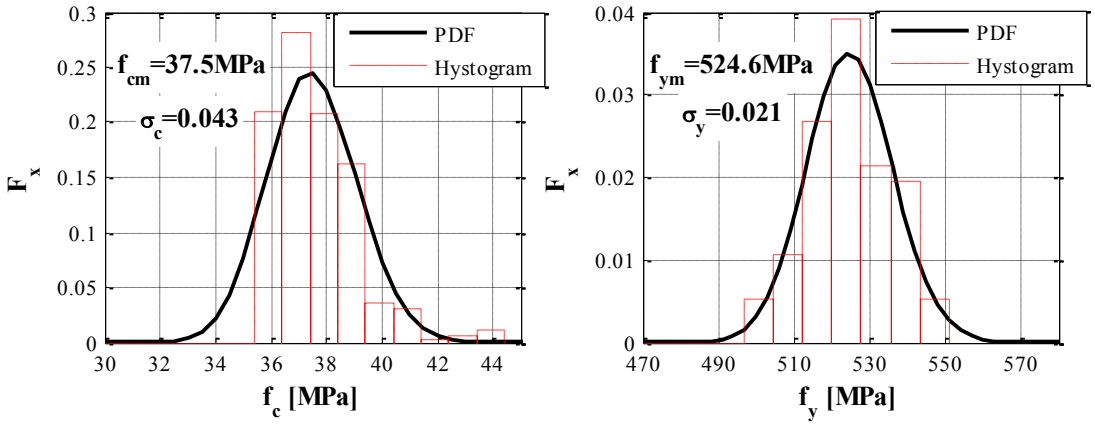

(a) Concrete compressive strength (b) Yielding strength of the steel

Fig. 4 Statistical distributions of the experimental tests

Compressive and tensile experimental tests were performed on concrete and reinforcement specimens, respectively. These tests are mandatory during the construction phase. The designer provided the results of these experimental tests and the corresponding statistical distributions are evaluated. Fig. 4 shows the lognormal distributions, fitting the PDFs (Probability Density Function) of both the concrete compressive strength and the yielding strength of steel bars. In this figure, the corresponding statistical parameters (mean and standard deviation) are also presented.

The mechanical properties of the masonry infills are evaluated considering the suggestion of the producer: the value of the shear cracking strength is equal to τ_o=0.28 MPa and the shear modulus is equal to G_w=2000 MPa.

3. Dynamic identification

An experimental dynamic identification test was performed on the investigated structure. The main goal of this experimental test is the definition of a reliable elastic analytical model of the investigated structure, i.e., closely representative of the actual distribution of mass and stiffness throughout the building as well as of its dynamic response.

The performed test aimed at the evaluation of the structure dynamic properties in operational conditions, i.e., no initial excitation or known artificial excitation were applied to the structure during the test. The dynamic identification test was performed when the structure was under construction. The structural elements (beams, columns and roof) were cast in-situ, as reported in Fig. 2, and the layout of the infill panels is shown in Fig. 3; no other nonstructural elements are in the structure at the testing time. As a consequence, the applied loads are the self-weight loads and the permanent nonstructural loads due to the infill panels; live loads are not present in the structure.

The investigated structure was instrumented at two levels (VI and VIII floor) with a couple of force balance accelerometers, 1-4 for the VIII floor and 5-8 for VI floor, as reported in Fig. 5, in the two main directions of the building in two opposite corners. These accelerometers are selected because of both their high sensitivity and their adjustable full-scale recording ranges (from ±0.25 g to ±4 g); these features make them capable to detect ambient vibrations (0-200 Hz). The location of the sensors was selected in order to get both the translational and torsional modes of the structure.

The identification of the modal parameters is performed according to different OMA (Operational Modal Analysis) techniques (Rainieri and Fabbrocino 2014, Rainieri *et al*. 2010, Rainieri *et al*. 2013), giving the results in terms of natural frequencies (Table 4) and modal shapes at the two monitored levels (Fig. 5).

Table 4 shows both the typology of the deformed shapes and the frequencies for the first three

Table 4 Experimental frequencies of the first three natural modes

Mode [-]	Type [-]	Natural frequency [Hz]
I	Translational (short side)	2.64
II	Translational (long side)+Torsion	4.01 (3.92 - 4.40)
III	Torsion	4.3 (4.2 - 4.4)

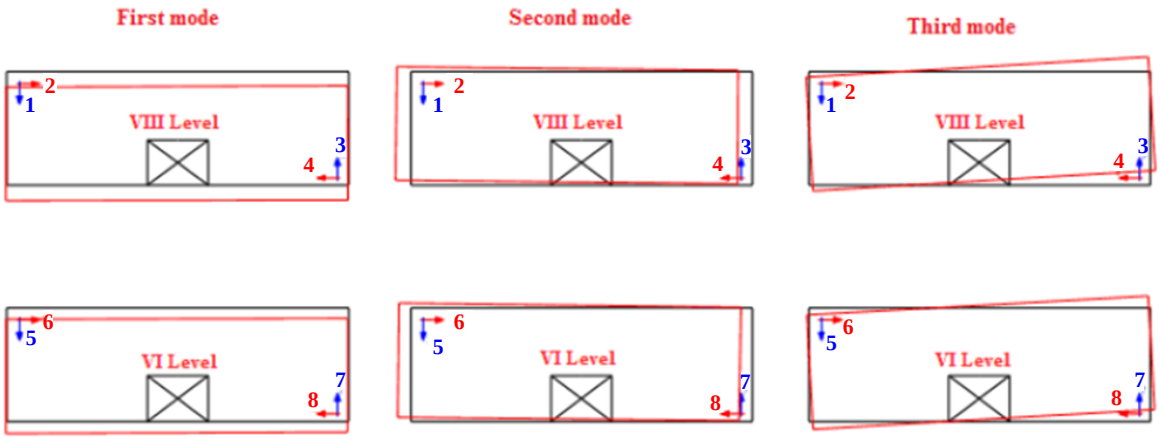

Fig. 5 Experimental modal shapes of the first three natural modes at the two monitored levels of the structure

modes; the confidence range of the last two modes is also reported.

The type of the modes is mainly translational along the short side for the first mode, translational along the long side and torsional for the second mode and mainly torsional for the third mode. The more flexible side of the structure corresponds to the *Y* direction (short side), i.e., the direction of the RC walls. This result can be justified by the distribution of the vertical resisting elements (columns and structural RC walls) (Fig. 2): most of the rectangular shaped columns have the long side along the *X* direction of the structure (long side).

In order to define the best fit model to the experimental dynamic properties, a parametric analysis is performed by means of linear modal analyses. An optimization process requires different steps, which are needed to:

i. define a reference structural model;

ii. define the uploading variables, i.e., the parameters that change in the study;

iii. perform numerical analyses with all the values of the uploading variables ranges (parametric study);

iv. choose the objective function to minimize.

The first step is performed in order to define the main structural features of the reference model for the following parametric study. Some different structural models are defined and their dynamic properties are investigated by means of modal analyses in order to evaluate their reliability in this specific case-study. In particular, the structural models are defined by considering some different structural hypotheses, that could influence the dynamic properties of structures. The study aims at defining the reference structural model by comparing the frequencies and the modal shapes of the structural models with the experimental results. The investigated models are:

- a Bare Model (BM), representative of the only RC structure (model.1 in Table 5 and in Fig. 6(a));

- a Bare Model with Concrete Panels (BMCP) at the underground stories (model.2 in Table 5 and in Fig. 6(b));

- two Infill Models (IM), without openings and with openings (model.3a and .3b, respectively, in Table 5 and in Fig. 6(c)).

The bare model#1 (BM) neglects the presence of the concrete and masonry panels and it only

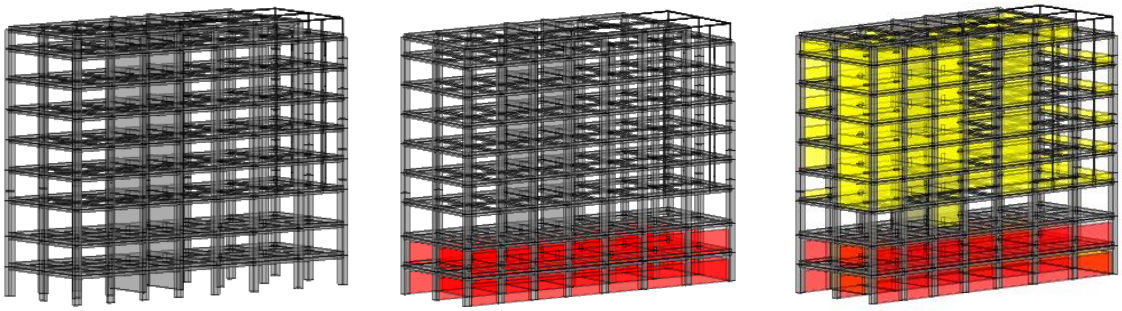

(a) Bare model (BM) - model #1 (b) Bare Model with Concrete Panels (BMCP) - model#2 (c) Infill Models (IM) - model#3

Fig. 6 Structural models for the optimization process

accounts for their mass. It is investigated since the influence of the infill panels could not be a priori defined. The RC structure consists of elastic beam elements: beam and column elements, RC walls (stair). The masses are concentrated in the mass center at each level and all the points of the floor are constrained with a rigid diaphragm in the *XY* plane.

The bare model#2 (BMCP) is also analyzed with the infill concrete panels (red panels in Fig. 6(b)) since the very high stiffness of these panels could have defined the global modal behavior of the structure.

The concrete (red panels in Fig. 6(c)) and masonry infill (yellow panels in Fig. 6(c)) panels are introduced in the RC structure model as an equivalent single diagonal strut. The equivalent diagonal strut is characterized by the elastic lateral stiffness of the panel, K_{el}, evaluated as in Eq. (1), according to (Fardis 1997)

$$K_{el} = G_w \cdot A_w / h_w \tag{1}$$

where A_w is the cross-sectional area of the infill panel, G_w is the elastic shear modulus of the infill material, and h_w is the clear height of the infill panel.

The presence of openings in the masonry panels (yellow panels in Fig. 6(c)) is also taken into account (model#3b) in order to evaluate the influence of this infill feature on dynamic properties of the case-study. For this model the stiffness of the panels is multiplied by a coefficient (Eq. (2)), linearly dependent on the opening ratio ($A_{openings} / A_{panel}$), based on the experimental results reported in Kakaletsis and Karayannis (2009)

$$\lambda_{openings} = \max\left(0;1-1.8\cdot\frac{A_{openings}}{A_{panel}}\right) \tag{2}$$

In the described structural models the mechanical characteristics of the materials are assumed according to the considerations of Section 2: the value of the concrete elastic modulus is assumed equal to E_c=31475 MPa and the shear modulus of masonry infills equal to G_w=2000 MPa.

The results of the modal analyses are reported in Table 5 in terms of frequencies and modal shapes of the first three modes for each model.

The bare model (model#1) results are very far from the vibration periods of the experimental tests, as expected: obtained frequencies are equal, on average, to 46% of experimental frequencies

Table 5 Investigated elastic structural models and results of the modal analyses

Models	Description	Mode 1	Mode 2	Mode 3	Freq. 1	Freq. 2	Freq. 3
[-]	[-]	[-]	[-]	[-]	[Hz]	[Hz]	[Hz]
1	Bare Model	Translational (long side) + Torsion	Torsion	Translational (short side)	1.36	1.73	1.85
2	Bare Model with Concrete Panels	Translational (long side)	Torsion	Translational (short side)	1.69	1.97	2.29
3a	Infill Model without openings	Translational (short side)	Translational (long side) + Torsion	Translational (long side)	2.91	4.07	4.56
3b	Infill Model with openings	Translational (short side)	Translational (long side) + Torsion	Translational (long side) + Torsion	2.83	3.91	4.53

(see Table 4).

The results obtained by considering the presence of concrete panels is slightly better, due to the increase in numerical frequencies of about 20% compared with model#1, but modal shapes are still quite far from experimental results.

On the other hand, the frequencies become more similar to the dynamic identification values (see Table 4) if both the presence of the masonry infills and the actual distribution of the openings are considered in the structural model. Frequencies are slightly higher than experimental values, on average, by 6% (see Table 4), and modal shapes of first three modes at monitored levels are very similar to the shapes provided by dynamic identification.

Hence, it is confirmed that the masonry infills as well as the presence of openings cannot be neglected when evaluating elastic dynamic properties of a RC building, as already discussed in literature (Ricci *et al*. 2011b).

Since the numerical linear model is defined (model#3b), the mechanical characteristic of the concrete and the masonry are investigated through an optimization process in order to closely match the experimental dynamic properties. The selected updating parameters are the elastic modulus of concrete, E_c, and the shear modulus of masonry, G_w.

By adopting a fine increment of the values of these two parameters, a total number of 451 modal analyses are performed by the "PBEE toolbox" software (Dolsek 2010), combining MATLAB® with OpenSees (McKenna and Fenves 2013).

Widely used objective functions are defined as function of the scatters between analytical and numerical values of natural frequencies, taking into account also the modal shape correlation (Rainieri 2008). In this paper the objective function is

$$J_M = \sum_{i=1}^{N_m} \left(\frac{|\Delta f_i|}{0.1} \right)^2 + \left(\frac{1 - MAC\left(\left\{ \psi_i^e, \psi_i^a \right\} \right)}{0.2} \right)^2 \quad (3)$$

$$\left|\Delta f_i\right| = \left|\frac{f_i^e - f_i^a}{f_i^e}\right| \tag{4}$$

$$\mathrm{MAC}\left(\left\{\psi_i^e, \psi_i^a\right\}\right) = \frac{\left|\left\{\psi_i^e\right\}^T \cdot \left\{\psi_i^a\right\}\right|^2}{\left\{\psi_i^e\right\}^T \cdot \left\{\psi_i^e\right\} \cdot \left\{\psi_i^a\right\}^T \cdot \left\{\psi_i^a\right\}} \tag{5}$$

The chosen objective function (Eq. (3)) consists of two terms: the scatter of frequencies (Δf_i) and the MAC value, defined in Eqs. (4)-(5), respectively. Both these two values are normalized with respect to the accepted limit value, i.e., a frequency scatter larger than 10% and a MAC value smaller than 0.8. In Eq. (4) f_i^e and f_i^a are the analytical and experimental frequencies of the structure for the i-th vibration mode, respectively; in Eq. (5) ψ_i^a is the analytical modal shape vector and ψ_i^e is the experimental modal shape vector of the i-th mode.

In Figs. 7(a)-(b) the two terms of the objective function are reported in order to highlight their efficiency when the limit values are exceeded. Fig. 7(c) shows the objective function versus the investigated mechanical properties. The local minimum values of the objective function are reported as white dots. The best local minimum point corresponds to E_c=32700 MPa and G_w=1900 MPa (quite similar to values adopted in preliminary evaluation of reference model).

The results of the modal analyses and the optimum values are showed in Table 6 in terms of frequency scatter and modal shape agreement. Fig. 8 shows the modal shapes of the first three modes for the best fit model. In this comparison the second analytical mode is compared with the third experimental mode and vice versa, according to their modal shapes. This assumption does not influence the goodness of the optimization study results since the hierarchy of these two modes is not clearly defined due to their very similar frequency values.

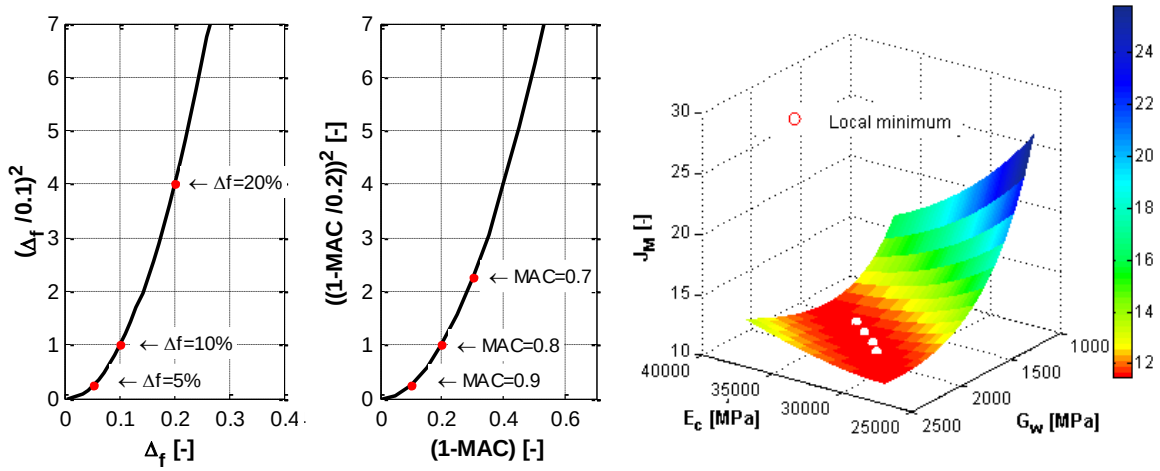

(a) First term of the objective function (J_M) in Eq. (3) versus the scatter of frequency in Eq. (4)

(b) Second term of the objective function (J_M) in Eq. (3) versus the scatter of frequency in Eq. (5)

(c) Objective function (J_M) versus elastic modulus of concrete (E_c) and shear modulus of masonry (G_w). The white markers are the local minimum of the objective function

Fig. 7 Results of the optimization process

Table 6 Results of the modal analysis on the model#5 with the optimal mechanical properties: frequencies, frequencies scatter and MAC values of the first tree modes

Mode [-]	Analytical frequency [Hz]	Frequency scatter [%]	MAC [-]
I	2.77	4.7	0.96
II	3.94	-9.2	0.86
III	4.56	12.0	0.82

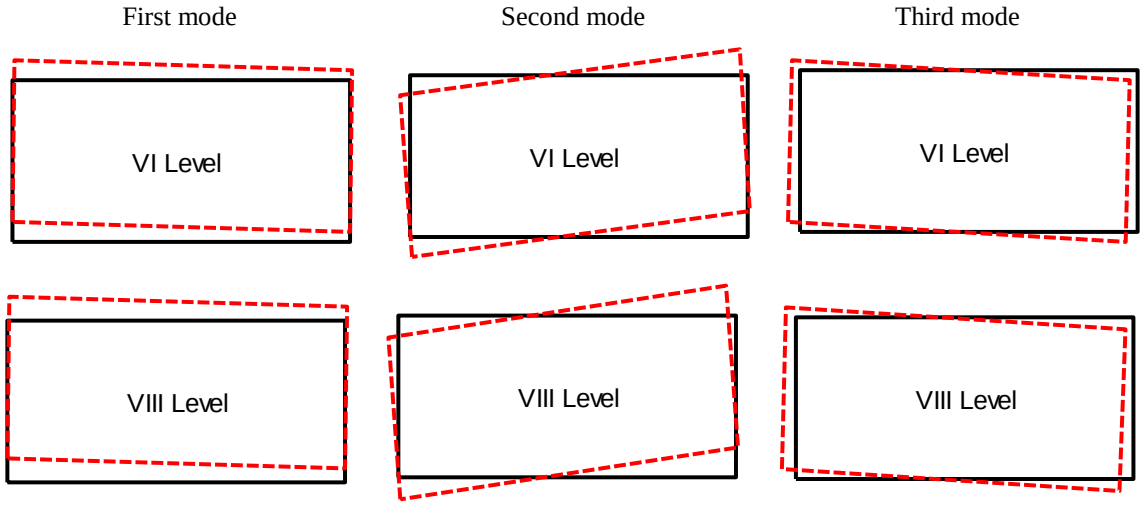

Fig. 8 Numerical modal shapes of the first three natural modes at the two monitored levels of the structure

It is worth to note that the first step (sensitivity study) of the optimization analysis could provide also other structural models by assuming other hypotheses and modelling refinements, such as the variation of rigid lengths of beams and columns joints, a more refined model of masonry infills, the flexibility of the foundation system. These assumptions should improve the frequency match. However, the computational effort could be useless since the already acceptable match of the modal analyses with the experimental results led the authors assume that the adopted structural model (#3) is acceptable for simulating the seismic response of the building. Moreover, the realistic values of the optimum mechanical properties of the materials also demonstrate that the influence of these neglected features should not be significant in the investigated case study.

4. Nonlinear analyses

Presence of infill can influence significantly the elastic dynamic properties of a RC building. From this point of view, the numerical-experimental comparison discussed in the previous Section is in line with the considerations reported in literature, e.g., in Ricci *et al*. (2011b), highlighting that the absence of infill elements in the numerical model may lead to errors up to 100% in the estimate of modal frequencies.

In this Section, the influence of infills on parameters defining seismic response and capacity of the case study building, too, is investigated.

In particular, pushover analyses are performed on the investigated structure in both the *X* and *Y* direction, with (Infilled Structure, IS) and without (Bare Structure, BS) modeling infills in order to investigate the influence of the masonry panels on the seismic response. The assumed lateral load pattern is proportional to the displacement shape of the first mode and the 5% accidental eccentricity is not considered (Magliulo *et al*. 2012).

For the structural elements a lumped plasticity model is used in the OpenSees-based analysis platform "PBEE toolbox" (Dolsek 2010), modified in order to include also infill elements (Celarec *et al*. 2012).

Three Limit States (LSs) are investigated: Damage Limitation (DL), Significant Damage (SD) and Near Collapse (NC) Limit States (LSs).

The definition of the criterion for the LS attainment is controversial and several definitions can be found in the scientific literature for both serviceability and ultimate limit states (a summary can be found in Kappos *et al*. (2006)). In this study, for the bare structure the DL LS is assumed to be attained when the first plastic hinge of RC elements yields. If a bare numerical model is used, seismic code (CEN 2005) suggests the use of a conventional displacement capacity (0.5% Interstory Drift Ratio - IDR, if the story has brittle nonstructural elements attached to the structure, as in the case of ordinary masonry infills), which is fictitiously higher than the actual deformation capacity of the infill wall. It should be ideally counterbalanced by the strength and stiffness contribution of infills, that are not accounted for in the bare numerical model. This approach is not adopted herein due to its "conventional" nature, whereas in the following the presence of infills and their influence on seismic capacity at DL is evaluated through an explicit modeling of these elements.

With regards to the infilled model, different assumptions can be found in literature regarding the attainment of the DL LS (Ricci *et al*. 2013). In this study, the DL LS conservatively corresponds to the reaching of the maximum resistance in the first infill (Colangelo 2012, Hak *et al*. 2012).

SD LS is assumed when the chord rotation capacity is equal to 3/4 of the ultimate chord rotation of the structural element. NC LS is defined as the attainment of the ultimate chord rotation in the first RC element, neglecting the achievement of shear failures in the elements. This definition should be justified a priori by considering the capacity design rule between shear and flexural strength in RC elements. In the following Sections, such strength hierarchy is checked through the comparison between the plastic shear and shear strength, evaluated according to the actual seismic code. This comparison allows excluding any brittle failure before the achievement of the ductile ones.

Concerning the infilled model, the results of the nonlinear analyses do not consider the possible shear failures due to infill-frame interaction in the critical zones (i.e., ends of the columns). Also in this case, a code-based assessment is carried out in order to exclude this kind of failure, thus validating such modelling hypothesis.

Hence, the overstrength at ultimate LSs is evaluated both in terms of seismic capacity, expressed as intensity measure of seismic action, and in terms of degree of safety concerning the possible activation of brittle failure mechanisms that should be avoided in RC building, designed according to a capacity design-based standard.

4.1 Nonlinear modeling

In the bare nonlinear model (BM) a lumped plasticity approach is adopted, i.e., nonlinear

flexural springs are inserted at the ends of the elastic elements.

In the columns, two independent nonlinear springs are assigned for each element end section, one for each orthogonal direction. Axial force-bending moment interaction is not considered at the plastic hinge even if the axial force excursion can influence the strength of the columns (Magliulo and Ramasco 2007). However, in this specific case, the global structural behavior should not significantly change, even because of the symmetry of the structure. Furthermore, this choice was justified by the use of a reference moment-rotation model, which easily allows identifying the different states of the plastic hinge.

For the multistory cantilever wall the yielding of the longitudinal reinforcement is expected to happen in the section at the base (no plastic hinges are expected in the upper stories).

The constitutive law of the moment-rotation end springs of the RC elements has three characteristic branches: a linear elastic first branch up to the cracking point, a linear branch from cracking to the maximum strength of the cross section and a perfectly plastic branch up to the ultimate point. The slope of the second branch is defined by the yielding point (θ_y, M_y). Section moment and curvature are calculated by means of a fiber section analysis, for an axial load value corresponding to gravity loads.

For beams, columns and concrete walls, the yielding, θ_y, and ultimate, θ_u, chord rotations are calculated according to the formulas proposed in Biskinis and Fardis (2010a) and in Biskinis and Fardis (2010b), respectively. For the concrete walls the shear-span is assumed equal to the entire height of the walls. According to these reference works, for beams and columns the yielding rotations is evaluated with Eq. (6), while for walls with Eq. (7), and the ultimate rotations of all RC elements are calculated according to Eq. (8)

$$\theta_y = \varphi_y \cdot \frac{L_s + a_v \cdot z}{3} + 0.0014 \cdot \left(1 + 1.5 \cdot \frac{h}{L_s}\right) + a_{sl} \cdot \frac{\varphi_y d_{bL} f_y}{8 \cdot \sqrt{f_c}} \tag{6}$$

$$\theta_y = \varphi_y \cdot \frac{L_s + a_v \cdot z}{3} + 0.0014 \cdot \left(1 + 1.5 \cdot \frac{h}{L_s}\right) + a_{sl} \cdot \frac{\varphi_y d_{bL} f_y}{8 \cdot \sqrt{f_c}} \tag{7}$$

$$\theta_u = a_{st}\left(1 - 0.43 a_{cy}\right)\left(1 + \frac{a_{sl}}{2}\right)\left(1 - 0.42 a_{w,r}\right)\left(1 - \frac{2}{7} a_{w,nr}\right)(0.3)^{\upsilon}\left[\frac{\max(0.01;\omega_2)}{\max(0.01;\omega_1)} f_c\right]^{0.225} 25^{\left[(\rho_w f_{yw})/f_c\right]} \tag{8}$$

The authors dismiss the definition of the symbols in the above mentioned equations that is reported in the reference works.

Modeling the infill panels is a challenging goal because of several reasons, e.g., the variable nature of the material and the presence and modeling of openings: several researchers attempted to propose models of the infill walls for nonlinear analyses (Asteris *et al*. 2013).

In this paper the infill panels are modeled by means of equivalent struts. The adopted model for the force-displacement curve consists of four branches (Panagiotakos and Fardis 1996). The elastic behavior (Fardis 1997) is assumed up to the shear cracking strength (green point in Fig. 9), given by the product between the shear cracking strength and the cross-section area of the infill panel. After the first cracking, the behavior is defined by the maximum strength (F_y point in Fig. 9), assumed equal to 1.3 times the cracking strength, and the corresponding displacement (Δ_y point in Fig. 9), assuming that the secant stiffness up to this point is given in Mainstone (1971). The third degrading branch, with a negative stiffness equal to 0.01 times the elastic one, moves from the

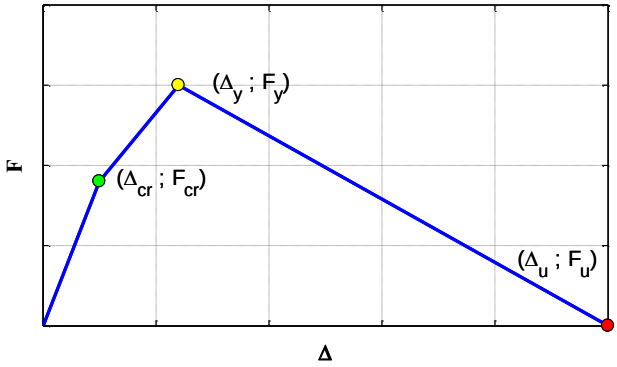

Fig. 9 Force-displacement relationship of the diagonal struts (under compression)

peak point to the residual strength value (red point in Fig. 9), assumed equal to 1% of the maximum strength.

The strength and deformation of the structural and nonstructural elements (RC elements and masonry panels) are evaluated with the mean values of the materials mechanical characteristics (see Fig. 4).

4.2 Results

In the following Section, the results of the nonlinear pushover analysis are reported for both the case of bare and infilled models. The N2 method (Fajfar and Gaspersic 1996, Kilar and Fajfar 1997b) is adopted in order to obtain the seismic capacity of the case study structure. The simplified pushover method is adopted as a standard code method. However, this assumption can be questionable since the case study is a medium-high rise building and the effect of higher modes can be significant. Several studies were performed in the last decades in order to extend the applicability of pushover methods to irregular buildings in both vertical (Delallera and Chopra 1995, Kilar and Fajfar 1997a) and plan direction; however, reliable applications to irregular building structures still have to be improved and validated. Moreover, according to some previous researches, the higher modes can influence the drift response only at the upper levels of medium-high or high structures with very long vibration periods (Kreslin and Fajfar 2011), i.e., in cases quite different with respect to the investigated building.

4.2.1 Bare structure

The pushover curves of the bare model (BM) in both the main directions are reported in Fig. 10(a) and in Fig. 11(a) in terms of total base shear, V, and roof displacement, Δ.

On this curve the first plastic hinge attainment (DL LS - yellow marker), the attainment of both the SD chord rotation (SD LS - orange marker) and the ultimate rotation in RC element (NC LS - red marker) are reported. The black point on the pushover curve indicates the values of the base shear and roof displacement for which a plastic mechanism (PM) is reached. In particular, a mechanism involving all the stories in *X* and *Y* direction, i.e., a global mechanism, is exhibited in both the directions. The achievement of the plastic mechanism is determined by observing the distribution of the yielded plastic hinges in RC elements (beams, columns and walls). In particular, the attainment of the yielding limit in these elements is evaluated and the achievement of a

collapse mechanism in one frame is assumed as the achievement of the structural collapse mechanism.

Fig. 10(b) and Fig. 11(b) show the story drift distribution along the height for the three considered limit states. In *X* direction the first yielded element is a longitudinal beam at the fifth floor and the first collapsed element is a longitudinal beam at the third floor. In *Y* direction the first yielded element is a beam at the second floor while the wall at the base reaches the ultimate rotation.

According to the N2 method (Fajfar and Gaspersic 1996), the capacity curve (black solid curve in Fig. 12 and in Fig. 13) and the idealized elastic-perfectly plastic force-displacement relationship

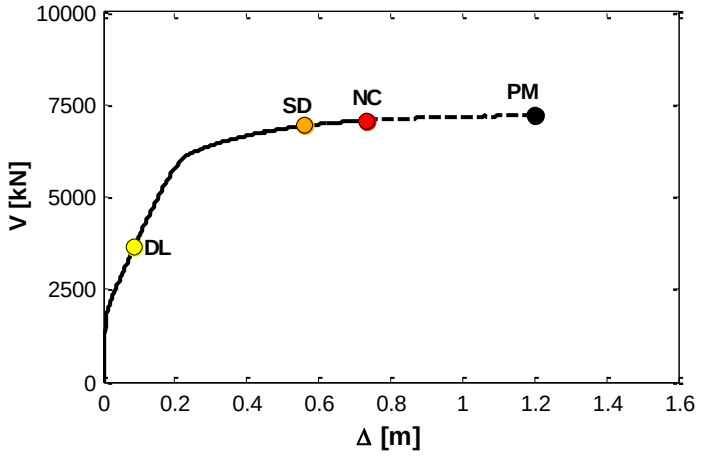

(a) Pushover curves in terms of total base shear and top displacement

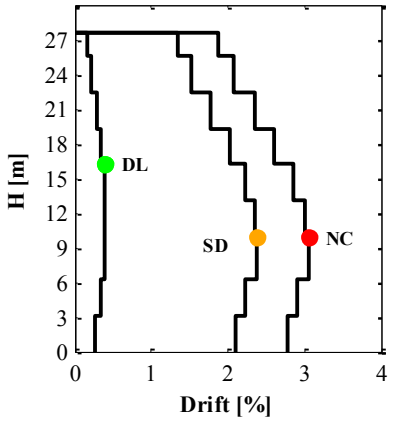

(b) Story drift for the BM at the DL, SD and NC LSs

Fig. 10 Results of pushover analysis for the BM in *X* direction

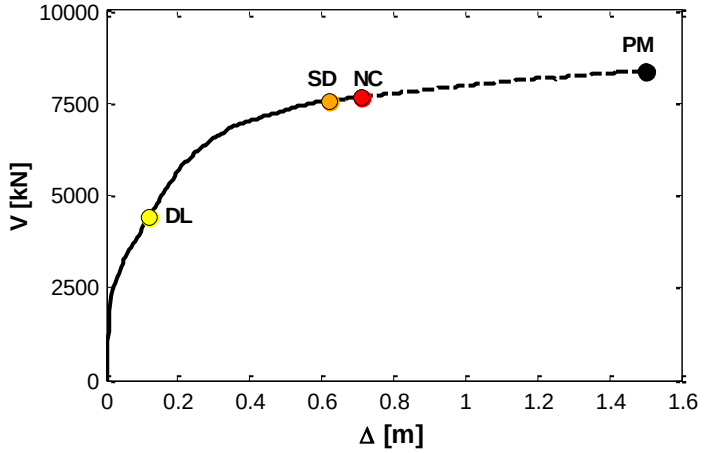

(a) Pushover curves in terms of total base shear and top displacement

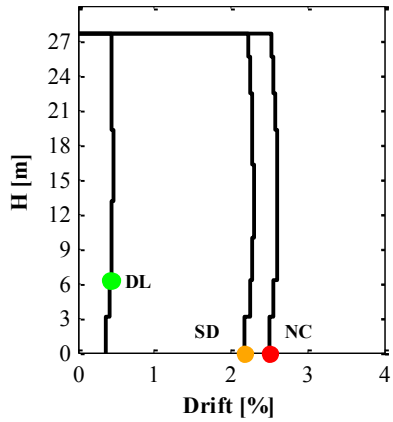

(b) Story drift for the BM at the DL, SD and NC LSs

Fig. 11 Results of pushover analysis for the BM in *Y* direction

of the equivalent SDOF (Single Degree Of Freedom) are evaluated (red solid curve in Fig. 12 and in Fig. 13).

The capacity curve is obtained by dividing the roof displacement and the base shear of the MDOF (Multiple Degree Of Freedom) system by the modal participation factor (Γ_x=1.55 and Γ_y=1.41). The base shear is then divided by the equivalent mass (m^*_x=1553t and m^*_y=1824 t) and by g in order to obtain the spectral inelastic accelerations, S_a.

The bilinear curve is obtained according to Eurocode 8 (CEN 2005), i.e., assuming the yield force equal to the base shear force at the NC LS and defining the initial stiffness of the idealized system in order to match the area below the capacity curve with the area of the idealized bilinear curve.

The effective period, T_{eff}, of the structure is 1.44 sec in X direction and 1.61 sec in Y direction.

The strength of the structure and the displacement capacity in the two considered directions are very similar at the three LSs; although the presence of the concrete walls in the Y direction, the most of the vertical resistant elements (columns) are oriented along the X direction.

Considering the results of the pushover analysis of the bare structure, some considerations can be drawn about the seismic design of new buildings according to the actual seismic code.

The design spectral acceleration is reported in Fig. 12 and in Fig. 13 (blue solid line) and it is obtained according to the code design spectra, considering the design periods of the structure and the adopted behavior factor, assumed by the designer. The overstrength of the structure can be evaluated as the ratio of this design value and the spectral acceleration at which the first hinge yields (yellow point in Fig. 12 and in Fig. 13). This value is equal to 1.52 in X direction and to 1.71 in Y direction.

According to Fardis (2009), this overstrength can be mainly justified by some aspects, as the expected difference between the mean and the design material strength, the limiting minimum code reinforcement requirements and some assumed simplifications in the design phase (e.g., the use of the same reinforcement in different cross-sections and the rounding-up of the number and/or diameter of reinforcing bars). The same author states that the value of this overstrength can be approximately estimated as 1.5, close to the value found in the investigated structure.

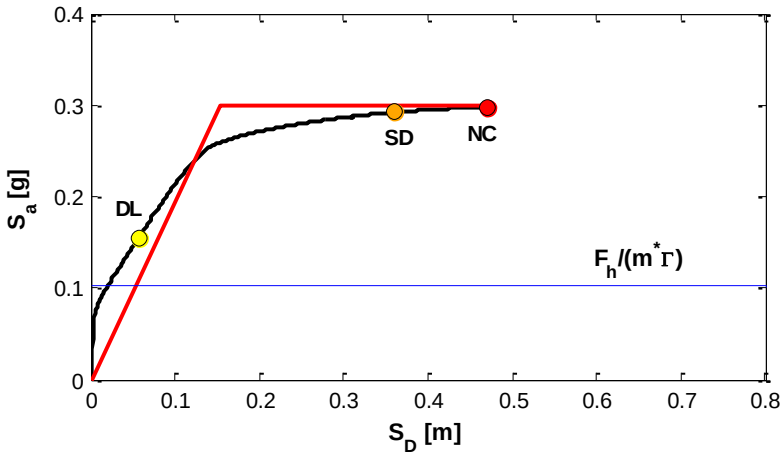

Fig. 12 Capacity curve (black solid line) of the equivalent SDOF for the BM with the three limit states and the design value of the acceleration (blue solid line) along with the bilinear curve (red solid line) in X direction

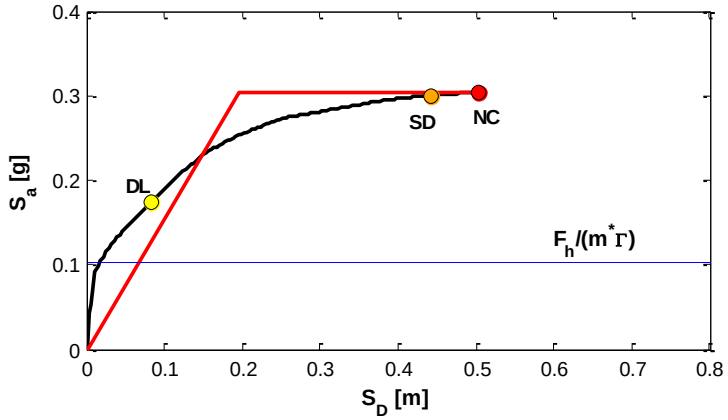

Fig. 13 Capacity curve (black solid line) of the equivalent SDOF for the BM with the three limit states and the design value of the acceleration (blue solid line) along with bilinear curve (red solid line) in *Y* direction

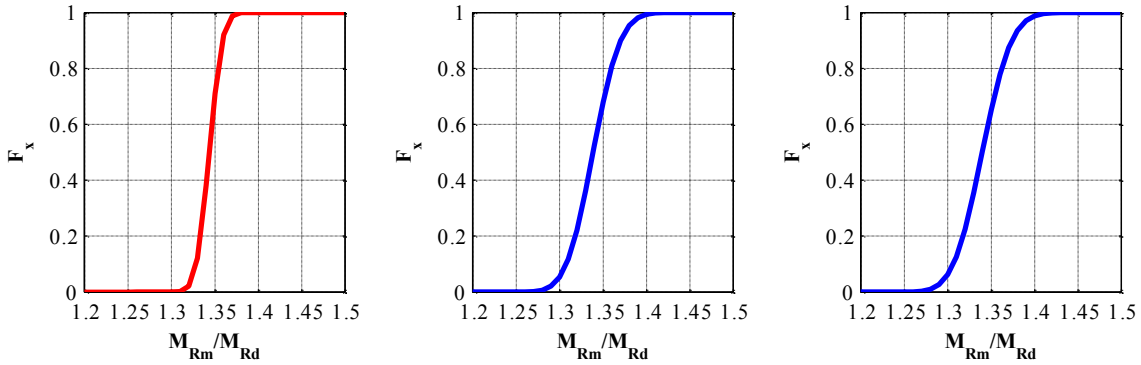

(a) Beams (b) Columns around *X* direction (c) Columns around *Y* direction

Fig. 14 CDF (Cumulative Density Function) distribution of the overstrenght ratios

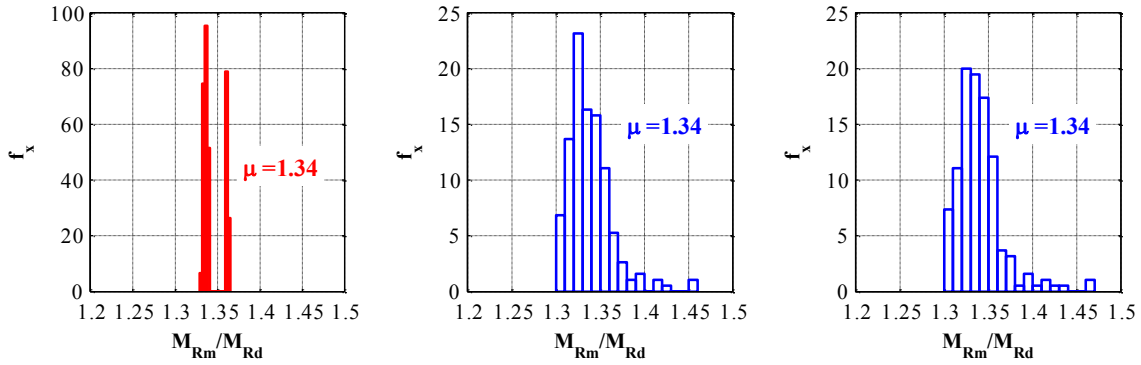

(a) Beams (b) Columns around *X* direction (c) Columns around *Y* direction

Fig. 15 PDF lognormal distribution of the overstrenght ratios

In Fig. 14 and in Fig. 15 the flexural overstrength, assumed as the ratio between mean and

design values of the material mechanical characteristics for beams and columns, are reported. The overstrength ratios are calculated as the ratios between the resistant moments (M_{rm}) in the RC elements evaluated with the mean values of materials strength (see Section 2) and the ultimate moments (M_{rd}) evaluated with the design strength of steel and concrete. The median overstrength value due to materials is equal to 1.34 for beams and columns.

In order to compare the seismic capacity of the structure with the design demand, the IN2 method (Dolsek and Fajfar 2004a) is applied for the equivalent SDOF systems, assuming as intensity measures the elastic spectral acceleration at the period of the equivalent SDOF system ($S_{ae}(T_{eff})$) and the Peak Ground Acceleration (*PGA*).

The IN2 method is a nonlinear method for the determination of an IM-EDP relationship, approximately representing an IDA (Incremental Dynamic Analysis) curve, starting from the N2 method results and defining the inelastic spectra through appropriated *R*-μ-*T* relationship. Since the lateral response is not characterized by a strength degradation, the simple *R*-μ-*T* relationship in Eqs. (9)-(10) are used, where T_C is the corner spectral period at the considered level of seismic intensity.

$$R = (\mu - 1)\cdot\frac{T}{T_C} + 1 \qquad T < T_C \tag{9}$$

$$R = \mu \qquad T \geq T_C \tag{10}$$

Since the seismic performance of the structure have to be determined also at low intensity demand, that is for acceleration lower than the yield acceleration ($S_{a,y}$) of the idealized capacity curve, the IN2 curve is obtained approximating the first part of the IN2 curve with a bilinear curve (Dolsek and Fajfar 2005). The two parts of the bilinear curve are separated by the point (D_e, F_e), which represents the boundary of the initial ideal elastic behavior. It is arbitrarily defined as the point where the stiffness is equal to 95% of the initial stiffness. The ductility and the reduction factor for this part of the curve (R<1) is defined in Eq. (11)

$$\mu = \begin{cases} \dfrac{\mu_e R}{r_e} & R < r_e \\ \dfrac{R - r_e}{1 - r_e}(1 - \mu_e) + \mu_e & r < R < 1 \end{cases} \tag{11}$$

In Eq. (11) $\mu_e=D_e/D_y$ and $r_e=F_e/F_y$, where D_y and F_y are the corner displacement and the maximum force of the idealized bilinear curve.

The IN2 curve for the bare structure are reported both in terms of elastic spectral acceleration (Fig. 16) and of *PGA* (Fig. 17) with the three seismic intensity levels. In order to assess the seismic performance of the studied building and to compare the response in the two main directions, the results of the pushover analyses and the design demand are also reported in Table 7.

The seismic capacity in *X* and *Y* direction is quite similar: only in terms of elastic spectral acceleration the lower effective period in *X* direction gives an increase of strength equal to 13%.

The displacements at the considered limit states are quite similar, but in *Y* direction a larger displacement capacity is generally observed.

Concerning the capacity at the DL LS, the *PGA* for which the attainment of the yielding in the first RC element is larger than the demand ($\overline{PGA}_{DL}$). The structure is safe at this LS also if the

displacement capacity is defined according to the achievement of the conventional "equivalent" IDR limit (0.5%), as discussed above (see PGA_{005}).

The seismic capacity of the building is greater than the demand at the SD and NC LSs. Also for this case study it is verified that the design according to the code elastic analysis is more conservative with respect to the safety verification performed by nonlinear static analysis (Magliulo *et al*. 2007).

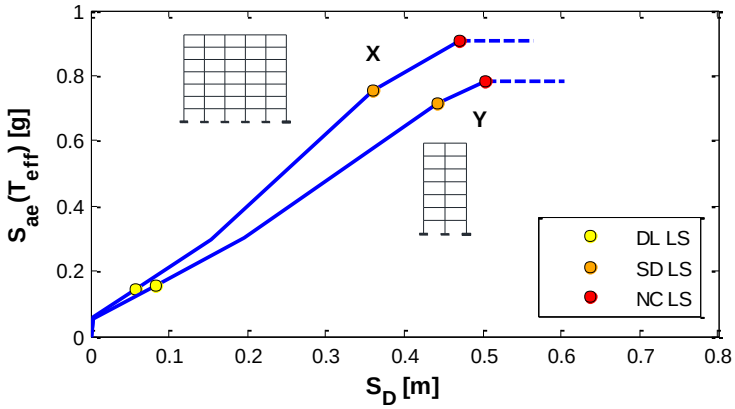

Fig. 16 IN2 curve (blue line) in terms of elastic spectral acceleration in *X* and *Y* direction with the three limit states for the BM

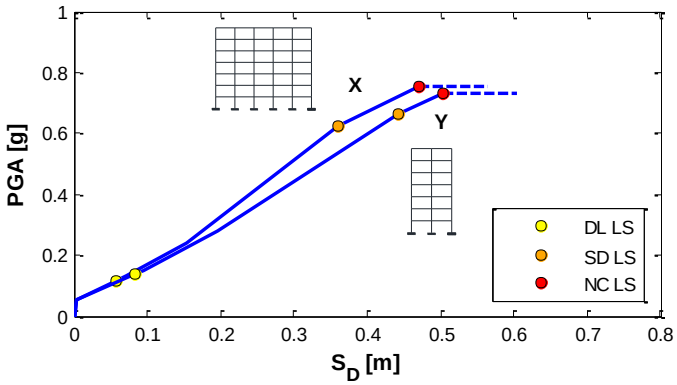

Fig. 17 IN2 curve (blue line) in terms of PGA in *X* and *Y* direction with the three limit states and the demand for the BM

Table 7 Nonlinear analyses results in *X* and *Y* direction for the BM

	Capacity - SDOF							Demand - SDOF						
Mod.	S_D NC	S_D SD	S_D DL	S_a Y	S_{ae} NC	S_{ae} SD	S_{ae} DL	PGAN C	PGAS D	PGAD L	PGA005	$\overline{\text{PGAN}}$ C	$\overline{\text{PGAS}}$ D	$\overline{\text{PGAD}}$ L
[-]	[m]	[m]	[m]	[g]	[g]	[g]	[g]	[g]	[g]	[g]	[g]	[g]	[g]	[g]
X	0.47	0.36	0.056	0.30	0.90	0.75	0.14	0.75	0.63	0.12	0.13	0.33	0.28	0.10
Y	0.51	0.44	0.084	0.30	0.78	0.72	0.16	0.73	0.66	0.14	0.15	0.33	0.28	0.10

4.2.2 Infilled structure

In this Section the results of the pushover analyses are reported for the infilled model (IM) in both the main directions of the structure.

Fig. 18(a) shows the pushover curve in *X* direction for both the bare (gray line) and the infilled model (black line). At the NC LS (red dot) the collapse mechanism is not reached but it is clearly close to involve 7 stories of the structures. The DL LS corresponds to the attainment of the maximum strength in the first infill, that occurs at the fourth level. The first yielded RC element is a beam at the 3rd level and the first failed element is a beam at the 5th level (Fig. 18(b)).

Fig. 19(a) shows the pushover curve in *Y* direction for both the bare (gray line) and the infilled model (black line). At the NC LS the collapse mechanism is not reached but it is clear that it is close to involve all the stories of the structures. The DL LS corresponds to the attainment of the

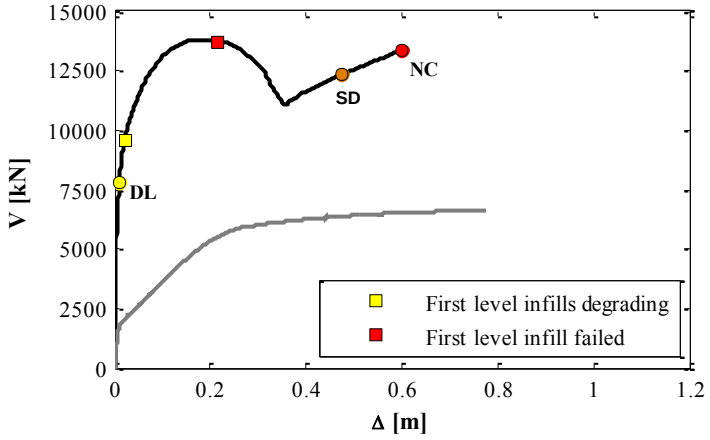

(a) Pushover curves in terms of total base shear and top displacement

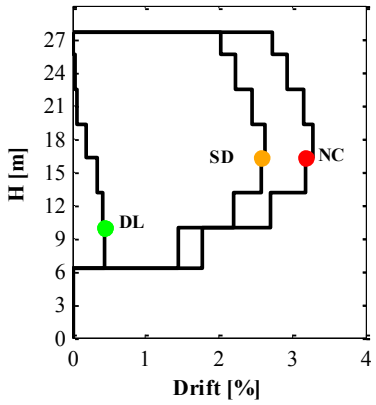

(b) Story drift for IM at the DL, SD and NC LSs

Fig. 18 Results of pushover analysis for the BM in *X* direction

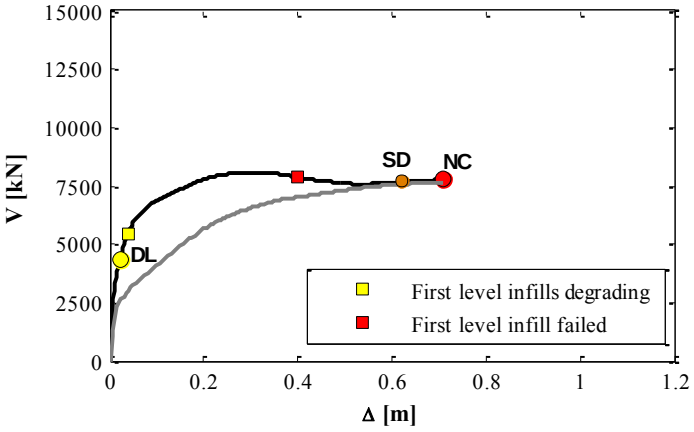

(a) Pushover curves in terms of total base shear and top displacement

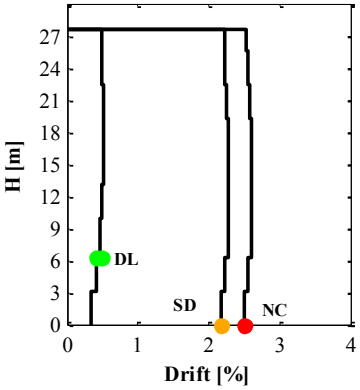

(b) Story drift for IM at the DL, SD and NC LSs

Fig. 19 Results of pushover analysis for the BM in *Y* direction

maximum strength in the first infill, that simultaneously occurs at the 4th and 5th floors. The first yielded RC element is a beam at the 2nd level and the first failed element is the wall at the base (Fig. 19(b)).

Fig. 20 and Fig. 21 show the results of the pushover analyses for the infilled structures: the capacity curve and the equivalent elastic-plastic SDOF.

Since the capacity curve of an infilled structure is characterized by a substantial decrease in strength after the infills begin to degrade, a multi-linear idealization is required (Dolsek and Fajfar 2005). The idealization procedure has to define three characteristic points, that correspond to the yielding, the initiation of degradation of the infills and the structural collapse. The idealized multi-linear curve is found by the following steps:

- the point at the maximum strength is found on the capacity curve in terms of base shear and top displacement;
- the yielding force is assumed equal to the maximum one;
- the yielding displacement is determined by the equal energy rule, which is applied to the idealized system and the pushover curve from 0 to the maximum point;
- the maximum displacement is assumed equal to the top displacement of the structure at the NC LS;
- the residual strength of the last point is found by the equal energy rule, which is applied to the idealized system and the pushover curve from the maximum to the last point of the pushover curve.

The effective periods of the structure are 0.48 sec in *X* direction and 0.85 sec in *Y* direction.

According to the pushover and the capacity curves, the strength increase at ultimate LSs due to the presence of infills in *X* direction is larger than in *Y* direction due to the higher number of masonry panels in the former direction. In both directions the DL LS is achieved for very low values of displacement.

The displacement capacities are close in the two directions and the same conclusion can be drawn if the bare and the infilled models are compared.

Fig. 22 and Fig. 23 show the IN2 curve for both the directions. The intensity measure is assumed equal to the spectral acceleration (Fig. 22) and to the peak ground acceleration (Fig. 23) and both of them are reported versus the inelastic top displacement.

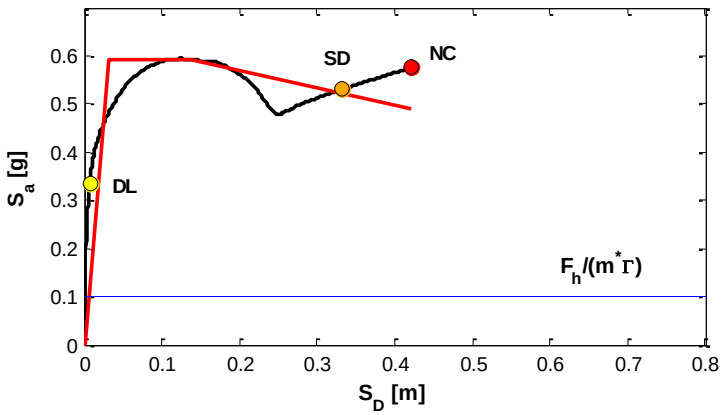

Fig. 20 Capacity curves (black solid line) of the SDOF equivalent system with the three limit states and the design value of the acceleration (blue solid line) along with the bilinear curve (red solid line) in *X* direction

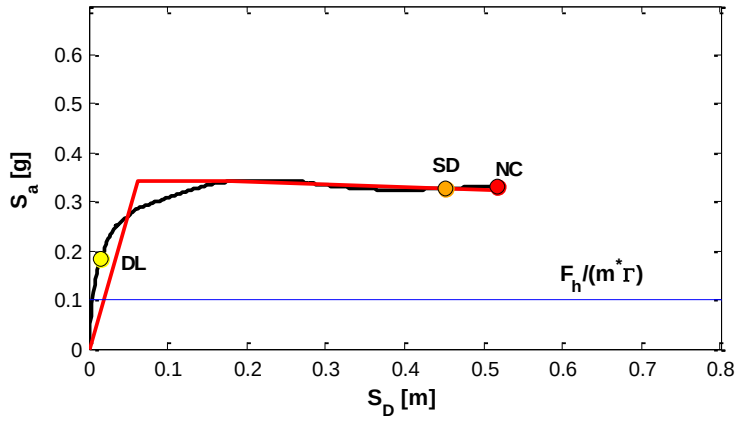

Fig. 21 Capacity curves (black solid line) of the SDOF equivalent system with the three limit states and the design value of the acceleration (blue solid line) along with the bilinear curve (red solid line) in *Y* direction

For infilled frames, Eqs. (9)-(10) are not appropriate and the specific *R*-μ-*T* relation, proposed in Dolsek and Fajfar (2004b), are used to obtain the IN2 curves in terms of elastic spectral acceleration. For the IN2 curves the initial part is defined again according to the procedure, reported for the bare model, that is defining the point (D_e, F_e) where the stiffness is equal to 95% of the initial one.

The mentioned differences in terms of inelatic spectral acceleration are also found in terms of elastic acceleration for the considered limit states. This result corresponds to higher values of PGA at ultimate LSs for *X* direction, although the difference is smaller due to the higher values of the effective periods in *Y* direction. The higher stiffness of the infilled model gives higher values of capacity in terms of S_a and in terms of PGA if compared to the bare models.

At ultimate LSs the safety factor is high in both the directions in terms of *PGA* (around 7 in *X* direction and 5 in *Y* direction). It is worth to underline that the beneficial effect of the infill panels can be achieved only if the interaction with the frame does not cause any brittle shear failure in the columns.

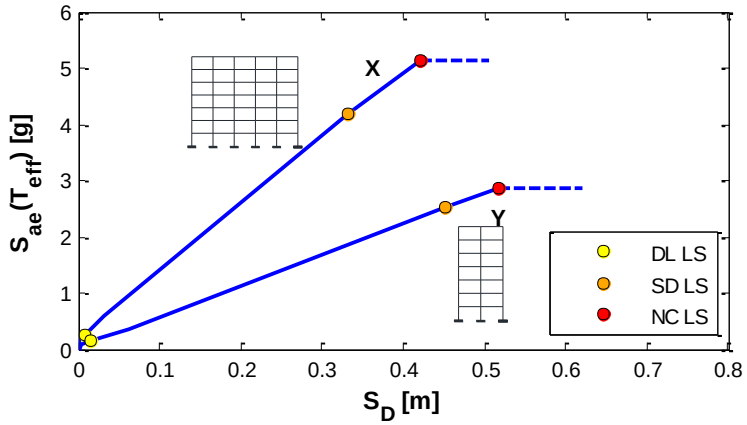

Fig. 22 IN2 curve (blue line) in terms of elastic spectral acceleration for the IM in *X* and *Y* direction

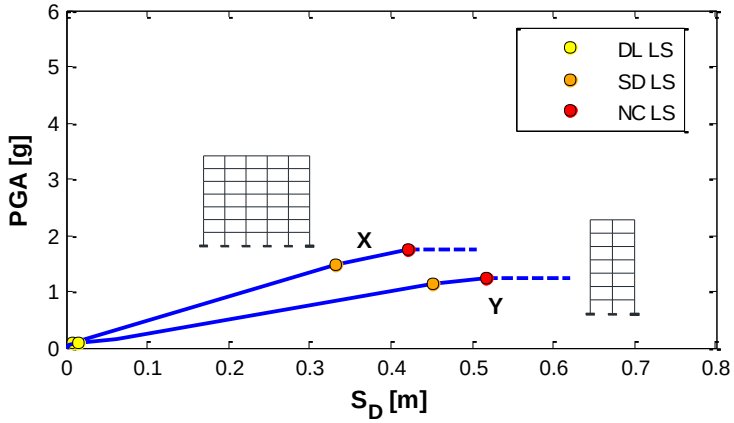

Fig. 23 IN2 curve (blue line) in terms of PGA for the IM in *X* and *Y* direction

Table 8 Results of N2 method for the IM in *X* and *Y* direction

Model	Capacity - SDOF							Demand - SDOF					
	$S_{D,NC}$	$S_{D,SD}$	$S_{D,DL}$	$S_{a,y}$	$S_{ae,NC}$	$S_{ae,SD}$	$S_{ae,DL}$	PGA_{NC}	PGA_{SD}	PGA_{DL}	$\overline{PGA}_{NC}$	$\overline{PGA}_{SD}$	$\overline{PGA}_{DL}$
[-]	[m]	[m]	[m]	[g]	[g]	[g]	[g]	[g]	[g]	[g]	[g]	[g]	[g]
X	0.42	0.33	0.007	0.57	5.12	4.19	0.26	1.76	1.12	0.075	0.33	0.28	0.10
Y	0.52	0.45	0.016	0.34	2.88	2.52	0.16	1.25	1.46	0.074	0.33	0.28	0.10

Concerning the DL LS, the safety factor for the DL LS is lower than 1. The actual seismic code provisions seem to be much more conservative for the ultimate LSs than for the DL LS, if the contribution of infills is explicitly taken into account. This can be explained by the influence of infills at DL. If their presence is explicitly taken into account, the displacement capacity strongly decreases, due to their brittle behavior that limits the deformation capacity corresponding to such performance level; on the other side, given equal the displacement capacity, the stiffness (and strength) of infills increases the seismic capacity compared with the bare frame. These effects tends to balance each other, but in some cases the former (detrimental) prevails over the latter (beneficial), leading to an overall reduction in seismic capacity at DL. This is likely to happen especially for medium/high rise new designed structure, when the stiffness contribution of infills to the bare frame is relatively low (Ricci *et al*. 2012a, Ricci *et al*. 2012b, Ricci *et al*. 2013).

4.3 Considerations on the seismic design according to the actual code

In the previously described pushover analyses, it is assumed that the shear capacity of the structural elements is adequate. In this Section, some considerations about this assumption are described.

The investigated case study was designed according to the seismic provisions required by Italian building code. The authors can assume that the shear capacity of the structural elements is adequate: shear failure mechanisms are avoided by adopting a capacity design philosophy. Moreover, the Italian code requires verifying the shear failure in columns if the height of the infill panel does not cover the entire height of the column.

According to the described design approach, two typologies of shear failure can still affect the seismic safety of the case study, as explained in the following.

1) Italian code does not provide any requirements in case the panel height is equal to the clear height of the column. In order to exclude shear failure in this case, the authors compare the seismic shear demand due to the panel-to-structure interaction with the shear strength of the vertical elements.

2) The efficiency of the capacity design rule can fail if the material overstrength overpasses the overstrength factor, adopted in the capacity design rule. The capacity/demand ratio for shear strength, evaluated with the expected (mean) material properties, provides a measure of the actual degree of safety for this kind of failure.

Another effect of the infill panel influence is related to the global response. As stated in the previous Sections, the infill can significantly increase both strength and stiffness of the structure. On the contrary, if the layout of these stiff elements is irregular along the structure (both in plan and in elevation), the global response could change in terms of failure mechanisms (soft-story mechanism) as well as damage distribution in the structural elements (localized seismic demand).

With regards to the potential local interaction between infill panels and RC elements (columns), the European code applies to buildings designed for DC H or M, no matter the structural system (wall or frame), some prescriptions, not included in the Italian code (D. M. 14/01/2008 2008a). In particular, to prevent failure of a column with a stiff and strong infill, the length of the column against which the diagonal strut bears should be verified in shear for the smallest of the following forces (V_{dem}):

a) the horizontal component of the strut force of the infill (V_{inf}), taken equal to the horizontal shear strength of the panel estimated from the shear resistance of bed joints;

b) the shear plastic force (V_{pl}), taking the clear length of the column as equal to the contact length and the column moment equal to twice the design value of the column flexural capacity. The contact length should be taken equal to the full vertical width of the diagonal strut of the infill, $w_{inf}/\cos\theta$, where θ is the angle between the horizontal and the panel diagonal. The width of the diagonal strut of the infill is evaluated according to the secant stiffness up to the truss maximum strength (Mainstone 1971). In the investigated structure this contact length is always included in the range [0.20-0.27] of the clear height of the panel and [1/6-1/5] of the length of the panel.

Fig. 24(a) and Fig. 25(a) show the ratios between these two values of the shear demand in the columns (above listed as “a” and “b” options) for both the directions (*X* and *Y*). In order to evaluate the shear safety of the columns, the ratios between the demand (V_{dem}), i.e., the minimum value between the above reported forces, and the shear strength (V_{str}) are also evaluated (Fig. 24(b) and Fig. 25(b)): at all the stories of the structure the shear failures of the vertical structural elements do not occur.

According to the Italian code the shear failures should be prevented by means of the capacity design rule. In order to avoid shear failure in beams, the demand is evaluated summing the shear due to the vertical loads and the shear forces induced by the development of the plastic hinges at the beam ends. This demand value is amplified by the overstrength factor (γ_{Rd}), assumed equal to 1.2 in ductility class “A” and 1.0 in ductility class “B”. For columns the demand is evaluated as the shear force due to the development of the plastic hinges at the column ends. The overstrength factor is assumed equal to 1.3 in ductility class “A” and 1.1 in ductility class “B”.

The difference between design and mean values of the material strength modifies the safety factors of this capacity design rule. In order to verify the modified overstrength ratios, the capacity design is checked both for beams and columns, considering mean and design strength.

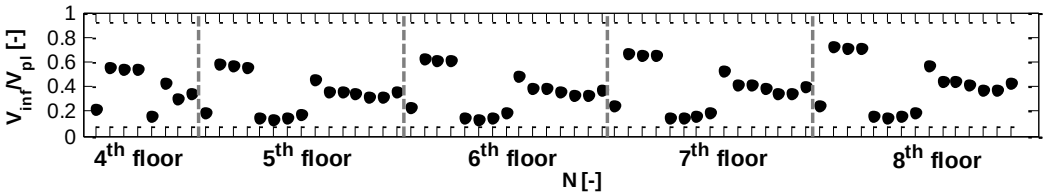

(a) Ratio between the horizontal component of the strut force of the infill and the plastic shear

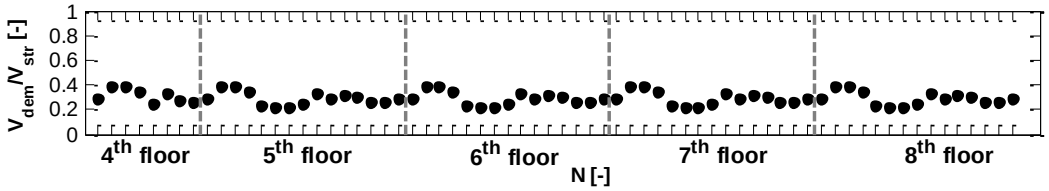

(b) Ratio between the demand and the shear strength

Fig. 24 Shear capacity of columns (X direction)

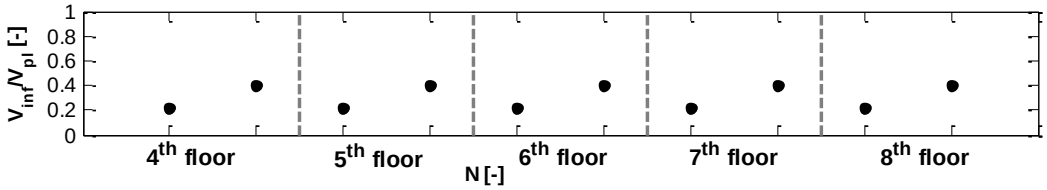

(a) Ratio between the horizontal component of the strut force of the infill and the plastic shear

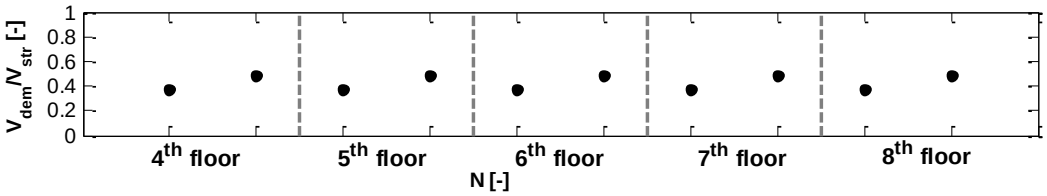

(b) Ratio between the demand and the shear strength

Fig. 25 Shear capacity of columns (Y direction)

Fig. 26 and Fig. 27 show the distribution of the expected overstrength ratio, defined as the ratio between the shear strength and the shear demand, obtained from the capacity design rule, both for beams and columns. This ratio is evaluated considering both the mean (red curves) and the design (blue curves) materials strengths. The data are fitted with a lognormal distribution.

In all the RC elements the overstrength ratios are larger than 1.0 and the design overstrength factors are larger than the corresponding values, provided by the code. Moreover, the adopted building code is safe-sided: the mean ratio values, reported in the figures, are larger than the values derived from the design.

In order to better investigate the overstrength ratio, the ratios between the expected (mean) shear strength (V_{Rm}) and the design shear strength (V_{Rd}) are evaluated in Fig. 28 for beams and in Fig. 29 for columns. In the same figures the ratio between the mean and design steel yielding strength (γ_s) and the ratio between the mean and design concrete compressive strength (γ_c) are also reported.

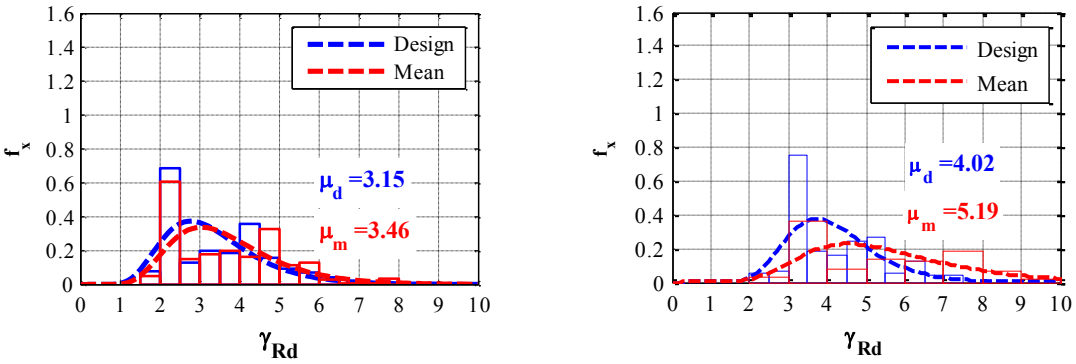

(a) Critical zone (b) Non critical zones

Fig. 26 Overstrength ratio distribution for shear of the beams in both the directions

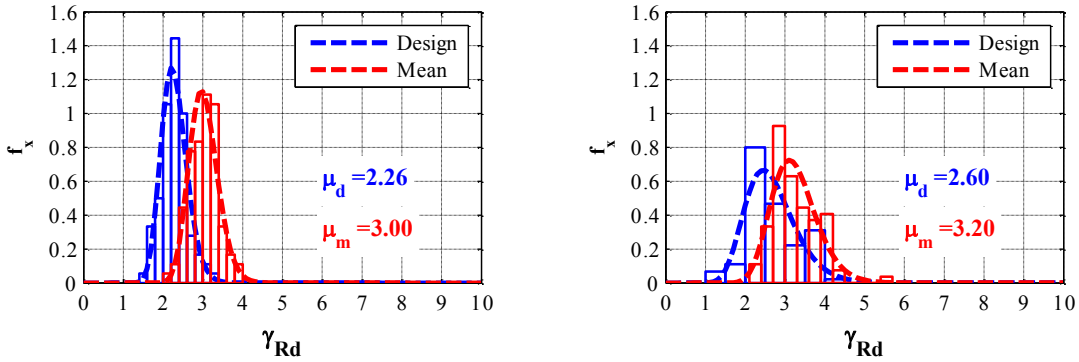

(a) X direction (b) Y direction

Fig. 27 Overstrength ratio distribution for shear in columns

The shear strength is evaluated according to the variable angle truss capacity model, provided by EC2; in particular, the shear strength of members with vertical shear reinforcement is evaluated as the smallest among the values in Eqs. (11)-(12). In these relationships θ is the angle between the concrete compression strut and the beam axis; its value should be limited between 1 and 2.5. All the remaining symbols in Eqs. (11)-(12) are reported in the reference code

$$V_{Rd,s} = \frac{A_{sw}}{s} \cdot z \cdot f_{ywd} \cdot \cot\theta \tag{11}$$

$$V_{Rd,\max} = \alpha_{cw} \cdot b_w \cdot z \cdot \upsilon_1 \cdot f_{cd} / (\cot\theta + \tan\theta) \tag{12}$$

From these shear strength formulas some simple considerations can be drawn. When $ctg\theta$ is in the range [1.0-2.5], the ratio between the mean shear strength and the design shear strength can be also evaluated by Eq. (14) and $ctg\theta$ is evaluated with Eq. (15). The strength ratio is highly influenced by the γ_c ratio and by the design value of transverse reinforcement mechanical ratio (ω_{swd}).

$$\frac{V_{Rsm}}{V_{Rsd}} = \gamma_s \sqrt{\frac{\frac{0.5 \cdot 1}{(\omega_{swd} \cdot \frac{\gamma_s}{\gamma_c})} - 1}{\frac{0.5 \cdot 1}{\omega_{swd}} - 1}} = \gamma_s \sqrt{\frac{\frac{0.5 \cdot 1}{\omega_{swd}} \frac{\gamma_c}{\gamma_s} - 1}{\frac{0.5 \cdot 1}{\omega_{swd}} - 1}} \tag{14}$$

$$\cot \theta_d = \sqrt{\frac{0.5 \cdot 1}{\omega_{swd}} - 1} \tag{15}$$

If $ctg\theta$ is larger than 2.5 in both the mean and design strength, their ratio is equal to the γ_s value, since it is equal to the ratio between the shear strength due to stirrups.

For non-critical zones in beams the ratios are equal or almost equal to γ_s. Such a result is justified by the value of $ctg\theta$ that is equal to 2.5 in most of cases and never lower than 2.0. For the critical zones of beams some higher values of ratios are recorded because of the smaller values of $ctg\theta$ caused by the larger value of transverse reinforcement mechanical ratio (see Eq. (14)).

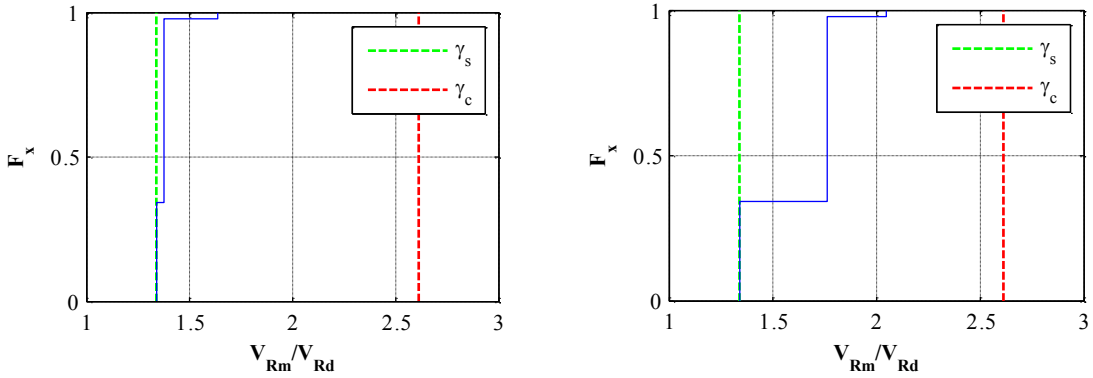

(a) Non-critical zones (b) Critical zones

Fig. 28 Ratios between the shear strength with mean and design materials strengths for beams

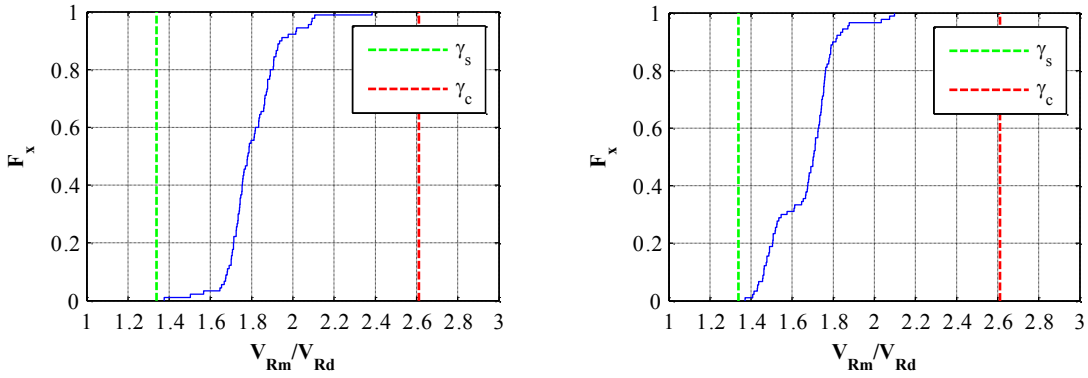

(a) *X* direction (b) *Y* direction

Fig. 29 Ratios between the shear strength with mean and design materials strengths for columns

Concerning the strength of columns in *X* direction, the value of $ctg\theta$ is included in the range [1-2.5]. Concerning the *Y* shear strength of columns, $ctg\theta$ is always equal to 2.5 for mean values and it is in the range (1.78-2.44) for design values. In this case smaller values of strength ratios are recorded with respect to the other direction. This is caused by the arrangement of the columns, that are mainly oriented along the X direction.

5. Conclusions

This paper describes the seismic assessment of a RC building by means of nonlinear static analyses. The case study is located in a high-medium seismic prone zone in Italy and it was designed according to a modern seismic code. The investigated structure has some interesting features, such as the presence of a dual structural typology in one direction (wall and frame systems) and an irregular layout of the infills along the height of the structure.

The definition of a reliable 3D structural model is a critical issue in evaluating the seismic performance of buildings under seismic actions. Many uncertainties can affect the outcomes of both linear and nonlinear analyses; moreover, the introduction of details and nonlinearities can significantly affect the analyses convergence as well as the capability of the model in describing the more severe damage state (i.e., the collapse mechanism). At this purpose, the work consists of a preliminary study aimed at the calibration of a reliable linear model of the structure. This study investigates the best-fit distribution (i.e., concrete walls at the underground level) and layout (e.g., presence of openings) of infill panels by a sensitivity analysis: the results of an in-situ dynamic identification test are compared with the dynamic properties of different linear models (i.e., frequencies and modal shapes). A parametric study was performed with the best-fit model in order define the optimum values of the materials mechanical characteristics (concrete and masonry). Both the good agreement of the model with the experimental results and the realistic optimum values of the material properties can let the authors neglect other modeling assumptions, e.g., foundation flexibility and openings location in the infill panels.

Structural nonlinearities are added to the best-fit model by a lumped plasticity approach and nonlinear static analyses are performed on both the bare and the infilled model. The safety of the structure is investigated at three seismic intensity levels: the near collapse (NC), the significant damage (SD) and the damage limitation (DL) limit states (LSs). The simplified pushover method is adopted as a standard code method. This assumption can be questionable since the case study is a medium-high rise building and the effect of higher modes can be significant. However, reliable applications to irregular building structures still have to be improved and validated, especially for the cases of dual systems and infilled structures.

Concerning the bare structure, the seismic safety is demonstrated for all the considered limit states in terms of both elastic spectral acceleration and PGA. At the NC LS and at the SD LS, the seismic response is still safe. Generally, the infills presence increases both stiffness and strength of the structures; on the contrary, it reduces the ductility due to the lower displacement capacity. In the investigated case, a global beneficial influence of infills is highlighted: no significant detrimental decrease of the displacement capacity is observed, since collapse mechanisms involving almost all the stories are observed, in both models and both directions. Moreover, the irregularity in elevation of the case study (infill layout along the height) lightly affects the structural response: soft-story mechanisms are not recorded during the analyses.

At the DL LS, the infilled model provides a low capacity: the failure of the infill panel is

observed for a low value of the seismic demand. In this case, the code design limitation on the story drift (0.5%) does not provide a safe-sided assessment. It is worth to note that such a consideration is influenced by the assumed failure at the DL LS in the infilled model, i.e., the attainment of the maximum strength in the first infill.

The above-described safety of the case study is related to a flexure-controlled behavior of RC members: the adopted model does not simulate either the shear failure in the elements or the local interaction with the infill panels. Indeed, according to the Italian construction code, the shear failure of the RC elements is prevented by adopting capacity design rules. However, the strength hierarchy could fail because of the material overstrength. In this study, in all the RC elements, the shear overstrength ratios obtained with the mean values are larger than the ratios obtained with the design values.

Concerning the infill interaction with the structure, the Italian code only requires the verification in case of short column effect (i.e., the panel height is smaller than the column one). Since no requirements are assumed in order to prevent shear failure due to the interaction of infill panels with columns, the specific Eurocode provisions are adopted and the absence of shear failures is a posteriori verified.

Acknowledgements

The authors would also like to acknowledge Prof. Eng. Giovanni Fabbrocino and Dr. Eng. Carlo Rainieri for the execution of the dynamic identification test campaign and for the valuable support during the analysis of the results.

References

Asteris, P.G., Cotsovos, D.M., Chrysostomou, C.Z., Mohebkhah, A. and Al-Chaar, G.K. (2013), "Mathematical micromodeling of infilled frames: State of the art", *Eng. Struct.*, **56**, 1905-1921.

Biskinis, D. and Fardis, M. (2010a), "Deformations at flexural yielding of members with continuous or lap-spliced bars", *Struct. Concrete*, **11**(3), 127-138.

Biskinis, D. and Fardis, M.N. (2010b), "Flexure-controlled ultimate deformations of members with continuous or lap-spliced bars", *Struct. Concrete*, **11**(2), 93-108.

Celarec, D., Ricci, P. and Dolsek, M. (2012), "The sensitivity of seismic response parameters to the uncertain modelling variables of masonry-infilled reinforced concrete frames", *Eng. Struct.*, **35**, 165-177.

CEN (2005), *Eurocode 8: design of structures for earthquake resistance - Part 1: general rules, seismic actions and rules for buildings, EN 1998-1*, Brussels, Belgium.

Colangelo, F. (2012), "A simple model to include fuzziness in the seismic fragility curve and relevant effect compared with randomness", *Earthq. Eng. Struct. Dyn.*, **41**(5), 969-986.

D. M. 14/01/2008 (2008a), *NormeTecniche per le Costruzioni*, G.U. n. 29 4 febbraio 2008. (in Italian)

D. M. 14/01/2008 (2008b), *NormeTecniche per le Costruzioni*, G.U. n. 29 4 febbraio 2008. (in Italian)

Delallera, J.C. and Chopra, A.K. (1995), "A simplified model for analysis and design of asymmetric-plan buildings", *Earthq. Eng. Struct.*, **24**(4), 573-594.

Dolsek, M. (2010), "Development of computing environment for the seismic performance assessment of reinforced concrete frames by using simplified nonlinear models", *Bull. Earthq. Eng.*, **8**(6), 1309-1329.

Dolsek, M. and Fajfar, P. (2004a), "IN2 - A simple alternative for IDA", *13th World Conference on Earthquake Engineering - Paper No. 3353*, Vancouver, Canada.

Dolsek, M. and Fajfar, P. (2004b), "Inelastic spectra for infilled reinforced concrete frames", *Earthq. Eng.*

Struct. Dyn., **33**(15), 1395-1416.
Dolsek, M. and Fajfar, P. (2005), "Simplified non-linear seismic analysis of infilled reinforced concrete frames", *Earthq. Eng. Struct. Dyn.*, **34**(1), 49-66.
Fajfar, P. and Gaspersic, P. (1996), "The N2 method for the seismic damage analysis of RC buildings", *Earthq. Eng. Struct. Dyn.*, **25**(1), 31-46.
Fardis, M.N. (1997), *Experimental and numerical investigations on the seismic response of RC infilled frames and recommendations for code provisions*, Report ECOEST-PREC8 No. 6. Prenormative research in support of Eurocode 8.
Fardis, M.N. (2009), *Seismic design, assessment and retrofitting of concrete buildings based on EN-Eurocode 8*, Springer Dordrecht Heidelberg London New York.
Fiore, A., Porco, F., Raffaele, D. and Uva, G. (2012), "About the influence of the infill panels over the collapse mechanisms actived under pushover analyses: Two case studies", *Soil Dyn. Earthq. Eng.*, **39**, 11-22.
Hak, S., Morandi, P., Magenes, G. and Sullivan, T.J. (2012), "Damage control for clay masonry infills in the design of RC frame structures", *J. Earthq. Eng.*, **16**, 1-35.
Kakaletsis, D.J. and Karayannis, C.G. (2009), "Experimental investigation of infilled reinforced concrete frames with openings", *ACI Struct. J.*, **106**(2), 132-141.
Kappos, A.J., Panagopoulos, G., Panagiotopoulos, C. and Penelis, G. (2006), "A hybrid method for the vulnerability assessment of R/C and URM buildings", *Bull. Earthq. Eng.*, **4**(4), 391-413.
Kilar, V. and Fajfar, P. (1997a), "Simple push-over analysis of asymmetric buildings", *Earthq. Eng. Struct.*, **26**(2), 233-249.
Kilar, V. and Fajfar, P. (1997b), "Simple push-over analysis of asymmetric buildings", *Earthq. Eng. Struct. Dyn.*, **26**(2), 233-249.
Kirac, N., Dogan, M. and Ozbasaran, H. (2011), "Failure of weak-storey during earthquakes", *Eng. Fail Anal.*, **18**(2), 572-581.
Kreslin, M. and Fajfar, P. (2010), "Seismic evaluation of an existing complex RC building", *Bull. Earthq. Eng.*, **8**(2), 363-385.
Kreslin, M. and Fajfar, P. (2011), "The extended N2 method taking into account higher mode effects in elevation", *Earthq. Eng. Struct.*, **40**(14), 1571-1589.
Magliulo, G., Maddaloni, G. and Cosenza, E. (2007), "Comparison between non-linear dynamic analysis performed according to EC8 and elastic and non-linear static analyses", *Eng. Struct.*, **29**(11), 2893-2900.
Magliulo, G., Maddaloni, G. and Cosenza, E. (2012), "Extension of N2 method to plan irregular buildings considering accidental eccentricity", *Soil Dyn. Earthq. Eng.*, **43**, 69-84.
Magliulo, G. and Ramasco, R. (2007), "Seismic response of three-dimensional R/C multi-storey frame building under uni- and bi-directional input ground motion", *Earthq. Eng. Struct. Dyn.*, **36**(12), 1641-1657.
Mainstone, F. (1971), "On the stiffnesses and strengths of infilled frames", *Proceedings of the Institution of Civil Engineering*, Supplement IV 57-90.
McKenna, F. and Fenves, G.L. (2013), *OpenSees Manual*, Pacific Earthquake Engineering Research Center
Mpampatsikos, V., Nascimbene, R. and Petrini, L. (2008), "A critical review of the RC frame existing building assessment procedure according to Eurocode 8 and Italian Seismic Code", *J. Earthq. Eng.*, **12**, 52-82.
Panagiotakos, T.B. and Fardis, M.N. (1996), *Seismic response of infilled RC frames structures*, 11th World Conference on Earthquake Engineering, Acapulco, México.
Rainieri, C. (2008), "Operational modal analysis for seismic protection of structures", Ph.D. Thesis, University of Naples Federico II, Italy.
Rainieri, C. and Fabbrocino, G. (2014), *Operational Modal Analysis of Civil Engineering Structures*, Springer Science+Business Media New York.
Rainieri, C., Fabbrocino, G. and Cosenza, E. (2010), "Integrated seismic early warning and structural health monitoring of critical civil infrastructures in seismically prone areas", *Struct. Hlth. Monit.*, doi: 10.1177/1475921710373296.

Rainieri, C., Fabbrocino, G. and Verderame, G.M. (2013), "Non-destructive characterization and dynamic identification of a modern heritage building for serviceability seismic analyses", *Ndt&E Int.*, **60**, 17-31.

Ricci, P., De Luca, F. and Verderame, G.M. (2011a), "6th April 2009 L'Aquila earthquake, Italy: reinforced concrete building performance", *Bull. Earthq. Eng.*, **9**(1), 285-305.

Ricci, P., De Risi, M.T., Verderame, G.M. and Manfredi, G. (2012a), "Influence of infill presence and design tyology on seismic performance of RC buildings: fragility analysis and evaluation of code provisions at Damage Limitation Limit State", *15th World Conference on Earthquake Engineering* - Paper No. 5836, Lisbon, Portugal.

Ricci, P., De Risi, M.T., Verderame, G.M. and Manfredi, G. (2012b), "Influence of infill presence and design tyology on seismic performance of RC buildings: sensitivity analysis", *15th World Conference on Earthquake Engineering* - Paper No. 5184, Lisbon, Portugal.

Ricci, P., De Risi, M.T., Verderame, G.M. and Manfredi, G. (2013), "Influence of infill distribution and design typology on seismic performance of low- and mid-rise RC buildings", *Bull. Earthq. Eng.*, **11**(5), 1585-1616.

Ricci, P., Verderame, G.M. and Manfredi, G. (2011b), "Analytical investigation of elastic period of infilled RC MRF buildings", *Eng. Struct.*, **33**(2), 308-319.

Uva, G., Porco, F. and Fiore, A. (2012), "Appraisal of masonry infill walls effect in the seismic response of RC framed buildings: A case study", *Eng. Struct.*, **34**, 514-526.

SA